Simonas Krotkus, Frederik Nehm, Robby Janneck, Shrujan Kalkura, Alex A. Zakhidov, Matthias Schober, Olaf R. Hild, Daniel Kasemann, Simone Hofmann, Karl Leo, Sebastian Reineke

Influence of bilayer resist processing on p-i-n OLEDs: towards multicolor photolithographic structuring of organic displays

Erstveröffentlichung in / First published in:

SPIE OPTO. San Francisco, 2015. Bellingham: SPIE, Vol. 9360 *[Zugriff am: 23.05.2019]*.

DOI: https://doi.org/10.1117/12.2080174

Influence of bilayer resist processing on p-i-n OLEDs: towards multicolor photolithographic structuring of organic displays

Simonas Krotkus, Frederik Nehm, Robby Janneck, Shrujan Kalkura, Alex A. Zakhidov, et al.

Simonas Krotkus, Frederik Nehm, Robby Janneck, Shrujan Kalkura, Alex A. Zakhidov, Matthias Schober, Olaf R. Hild, Daniel Kasemann, Simone Hofmann, Karl Leo, Sebastian Reineke, "Influence of bilayer resist processing on p-i-n OLEDs: towards multicolor photolithographic structuring of organic displays," Proc. SPIE 9360, Organic Photonic Materials and Devices XVII, 93600W (16 March 2015); doi: 10.1117/12.2080174

SPIE.

Event: SPIE OPTO, 2015, San Francisco, California, United States

Influence of bilayer processing on p-i-n OLEDs: towards multicolor photolithographic structuring of organic displays

Simonas Krotkus[a], Frederik Nehm[a], Robby Janneck[b], Shrujan Kalkura[b], Alex A. Zakhidov[b,c], Matthias Schober[b], Olaf R. Hild[b], Daniel Kasemann[a], Simone Hofmann[a], Karl Leo[a] and Sebastian Reineke[a]

[a]Institut für Angewandte Photophysik, Technische Universität Dresden, 01062 Dresden, Germany;
[b]Fraunhofer Institute for Organic Electronics, Electron Beam and Plasma Technology FEP, 01109 Dresden, Germany;
[c]Department of Physics, Texas State University, San Marcos, TX 78666, USA

ABSTRACT

Recently, bilayer resist processing combined with development in hydrofluoroether (HFE) solvents has been shown to enable single color structuring of vacuum-deposited state-of-the-art organic light-emitting diodes (OLED). In this work, we focus on further steps required to achieve multicolor structuring of *p-i-n* OLEDs using a bilayer resist approach. We show that the green phosphorescent OLED stack is undamaged after lift-off in HFEs, which is a necessary step in order to achieve RGB pixel array structured by means of photolithography. Furthermore, we investigate the influence of both, double resist processing on red OLEDs and exposure of the devices to ambient conditions, on the basis of the electrical, optical and lifetime parameters of the devices. Additionally, water vapor transmission rates of single and bilayer system are evaluated with thin Ca film conductance test. We conclude that diffusion of propylene glycol methyl ether acetate (PGMEA) through the fluoropolymer film is the main mechanism behind OLED degradation observed after bilayer processing.

Keywords: OLED, doped organic films, photolithography, hydrofluoroethers, bilayer processing

1. INTRODUCTION

Organic light-emitting diode (OLED) technology based on multilayered thin films of thermally evaporated small molecules has matured in the past decade, with applications ranging from smart phone or tablet displays to solid-state lighting.[1,2] However, further advances in the structuring techniques of OLEDs are required in order to fulfill its full potential in providing low-cost light sources on a large area substrates[3] as well as to open new opportunities for emerging sensor applications by monolithic integration of state-of-the-art OLEDs with organic transistors, photodiodes or solar cells.[4–7]

To date, evaporation using shadow mask is commonly used to structure vacuum deposited small molecule organic semiconductor devices.[8] However, it has severe limitations with respect to providing simple, high resolution and cost-effective integration of the devices on a large scale substrates. On the other hand, photolithography is a parallel, high resolution patterning technique with a well established infrastructure in inorganic semiconductor industry as well as in liquid crystal display technology, where it is implemented for the backplane and color filter patterning. Despite its numerous advantages, photolithographic patterning is rarely applied for planar integration of OLEDs. This is mainly due to the incompatibility between the organic semiconductors and organic or water-based etchants, developers and resists which are used in the processing steps of conventional photolithography. Hence, various modifications to photolithographic structuring of OLEDs were proposed, including dry processing using super-critical CO_2,[9] direct photo-patterning of polymers containing cross-linking groups,[10,11] use of protective metal films[12,13] or exploiting the orthogonality between highly fluorinated materials and organic semiconductors, by using photoresists[14] or light-emitting polymers containing highly fluorinated groups.[15]

Send correspondence to: simonas.krotkus@iapp.de

Organic Photonic Materials and Devices XVII, edited by Christopher E. Tabor, François Kajzar, Toshikuni Kaino, Yasuhiro Koike, Proc. of SPIE Vol. 9360, 93600W · © 2015 SPIE
CCC code: 0277-786X/15/$18 · doi: 10.1117/12.2080174

Due to their low contribution in polar and hydrogen bonding,[16] hydrofluoroether (HFE) solvents have been demonstrated to be compatible with a wide range of organic semiconductor materials.[14,17–20] Recently,[21] our group showed a photo-patterning of single color OLEDs using bilayer method combined with fluoropolymer processing in HFEs. The proposed approach was shown to exhibit all the advantages attributed to conventional photolithography. In addition, it provides the compatibility between organic semiconductors and the photolithographic processing steps. In this work, we investigate further steps necessary to achieve structuring of multicolor OLED arrays, as required for *e.g.* high quality illumination or display applications, by examining the performance of series of devices exposed to different lithographic processes.

2. EXPERIMENTAL

2.1 Photo-patterning Protocol

The simplified scheme of the photolithographic processing is depicted in Figure 1. A glass substrate with the pre-patterned indium tin oxide (**ITO**) anode (i) is subsequently covered by spin-coating of (ii) the fluorinated polymer film and (iii) the imaging resist layer (**AZ nLOF-2020**, AZ Electronic Materials GmbH). Fluoropolymer and imaging resist form 2.7 μm and 2 μm thick films, respectively. Mutual orthogonality between these two layers ensures that processing of the imaging resist does not alter the properties of the fluoropolymer and *vice versa*. The bilayer is patterned by (iv) exposing defined parts of the surface to the UV radiation (SF-100 broadband exposure system, Intelligent Micro Patterning) and subsequent (v) developing in the Tetramethylammonium hydroxide (**TMAH**) based developer (**ma-D 533 S**, Microresist technology GmbH). Subsequently, the pattern is transferred into the fluoropolymer layer by (vi) spin-etching in a HFE solvent (**Novec7100**, 3M). To ensure the removal of resist leftovers an additional O_2 plasma treatment is applied. During the transfer step imaging resist serves as an etching mask. Next, the OLED stack is deposited (vii) under ultra high vacuum (see below for details) on top of the pre-defined bilayer resist pattern. This procedure is followed by a lift-off in a fluorinated HFE solvent (viii), during which the parts of the OLED stack deposited on top of the given bilayer are removed yielding patterned organic layers.

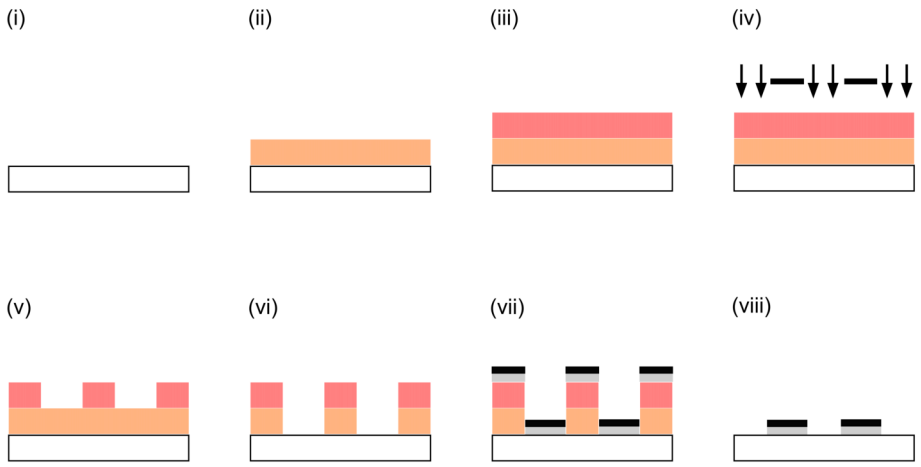

Figure 1. Simplified scheme of the photolithographic patterning procedure. (i) Substrate/electrode, (ii) spin-coat of the fluoropolymer, (iii) spin-coat of the imaging resist, (iv) UV exposure, (v) development of the imaging resist, (vi) development of the fluoropolymer, (vii) active layer deposition, (viii) lift-off in HFEs.

2.2 OLED Fabrication

Organic materials are commercially purchased and purified by vacuum gradient sublimation. Prior to device fabrication, the glass substrates coated with 90 nm thick ITO were cleaned using ultrasonic treatment in N-Methyl-2-pyrrolidon (**NMP**), distilled water, and ethanol. A single-chamber high vacuum tool (Kurt J. Lesker

Co.) is used for OLED device preparation. Organic and metal layers were thermally evaporated at a base pressure of 10^{-7} to 10^{-8} mbar without braking the vacuum. Evaporation rates and thicknesses of all layers are measured *in situ* via quartz crystals. Doping of organic film is achieved by co-evaporation. The organic layer sequence is based on the *p-i-n* device concept consisting of using doped charge transport layers, which enables low operational voltage and independent optimization of the device optics by varying transport layer thickness while maintaining the electrical performance.[22] The device is composed of hole and electron transport layers (HTL and ETL, respectively) which ensure efficient charge injection from the electrodes and subsequent charge transfer. The emission layer (EML) is then sandwiched between intrinsic electron and hole blocking layers (EBL and HBL, respectively), whose role is to confine injected charges and excitons within the emission layer. The stack architectures with optimized layer thicknesses for red- and green-emitting OLEDs[23] are depicted in Figure 2 (a) and (b), respectively. The red stack consists of 60 nm thick HTL formed of 2,2',7,7'-tetrakis-(N,N-dimethylphenylamino)-9,9'-spirobifluoren (**Spiro-TTB**, Lumtec) doped with 4 wt% 2,2'-(perfluoronaphthalene-2,6-diylidene)dimalononitrile (**F6-TCNNQ**, Novaled AG), 10 nm thick EBL of N,N'-di(naphthalen-1-yl)-N-N'-diphenyl-benzidine (**α-NPD**, ABCR), 20 nm thick EML composed of α-NPD doped with 10 wt% of the red phosphorescent emitter iridium(III)bis(2-methyldibenzo-[f,h]chinoxalin)(acetylacetonat) (**Ir(MDQ)$_2$(acac)**, Lumtec), 10 nm thick HBL of aluminum(III)bis(2-methyl-8-quninolinato)-4-phenylphenolate (**BAlq$_2$**, Sensient) and 60 nm ETL of 4,7-diphenyl-1,10-phenanthroline (**BPhen**, ABCR) co-evaporated with cesium (**Cs**, SEAS). The doping ratio of the ETL is adjusted to obtain a conductivity of 10^{-5}S/cm. The device is completed by depositing 100 nm layer of aluminum (**Al**, Kurt J. Lesker Co.) which serves as a cathode. The green OLED consists of 50 nm thick Spiro-TTB:F6-TCNNQ (4wt%) and BPhen:Cs as HTL and ETL, respectively. 10 nm thick layer of 2,2',7,7'-tetrakis-(N,N-diphenylamino)-9,9'-spirobifluorene (**Spiro-TAD**, Lumtec) and 10 nm BAlq$_2$ are used as EBL and HBL, respectively. EML consist of the phosphorescent green emitter Tris(2-phenylpyridine) iridium(III) (**Ir(ppy)$_3$**, Lumtec) incorporated into double matrix of 6 nm thick layer of 4,4',4"-tris(carbazol-9-yl)-triphenylamine (**TCTA**, Sensient) and 12 nm thick layer of 2,2',2"-(1,3,5-phenylen)tris(1-phenyl-1H-benzimidazol) (**TPBI**, Lumtec), with the doping concentration of 8 wt%. 100 nm thick Al layer is used as a cathode. In both OLED stacks the overlap between bottom ITO contact and metal cathode defines the active area of the device, which is 6.76 mm^2 and 10.20 mm^2 for devices defined via evaporation through the shadow mask and photo-patterned pixels, respectively. Electroluminescence spectra of vacuum deposited devices are shown in Fig. 2(c). After processing and lift-off, the OLEDs are encapsulated in nitrogen atmosphere using glass lids and UV-curing epoxy resin.

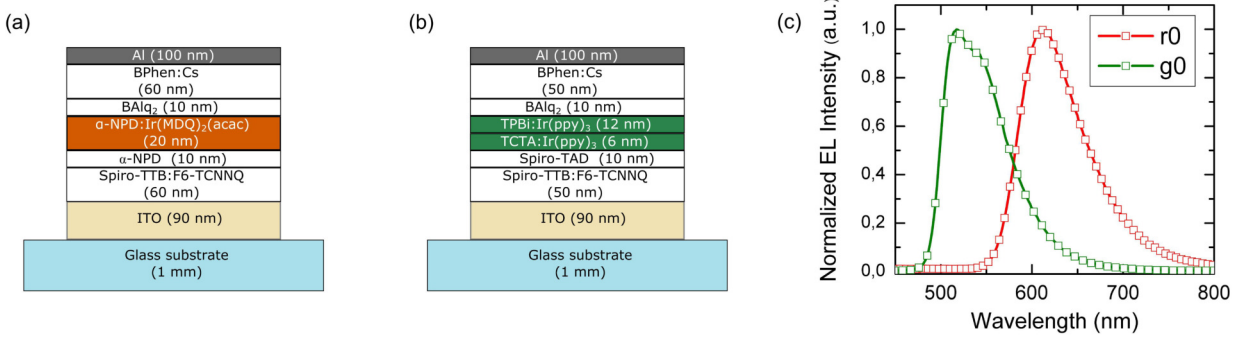

Figure 2. Standard electroluminescent devices used in this work: optimised red (a) and green (b) phosphorescent OLEDs comprising doped transport layers; (c) corresponding electroluminescence spectra of the reference devices (r0 and g0, respectively).

2.3 Device Characterization

All measurements of the encapsulated devices are carried out under ambient conditions. Current-voltage-luminance characteristics are measured using source measure unit (Keithley SMU 2400) and a calibrated Si-photodiode. The spectral radiance is recorded with a calibrated spectrometer (Instrument Systems GmbH CAS140). Efficiencies are calculated using Lambertian emission assumption. Luminance decay curves are acquired by aging OLEDs under constant current condition. The micrographs of electroluminescent pixels are taken using an optical microscope (Carl-Zeiss-Jena Jenaval).

2.4 Electrical calcium tests

Barrier evaluation of the coated polymers is done using electrical calcium tests. In this method, a thin, conducting, metallic calcium stripe reacts to non-conducting calcium hydroxide upon exposure to water. It is contacted electrically and acts as a sensor upon water ingress through the barrier, i.e. the investigated polymers. The quality of a moisture barrier is normally given by its water vapor transmission rate (WVTR), which is directly proportional to the derivative of the calcium's conductance over time.[24] The calcium sensor is contacted in a true four-point-probe conductivity measurement to avoid series resistance issues.[25] The Ca-Test stack consists of three layers, all of which are thermally evaporated in a multi-source evaporation system (Kurt J. Lesker Co.) at a base pressure of 10^{-8} mbar. Deposited onto a $2.5 \cdot 2.5$ cm^2 BK7 glass substrate (Schott, Mainz, Germany) are 100 nm of aluminum electrode fingers, 100 nm of calcium sensor (length: 11 mm, width: 5 mm), and 100 nm C_{60}. The latter is deposited over the whole sensor and acts as a mechanical decoupling of barrier and calcium.[26] Functional structuring of the evaporated layers was achieved by shadow masks placed in the evaporation path. Kapton tape is used to protect the samples' contact pads during spincoating deposition, which follows the evaporation process directly. All handling and processing before the measurement takes place in vacuum or in interconnected gloveboxes (MBraun, Garching, Germany). In the gloveboxes, an inert nitrogen atmosphere is kept with residual water and oxygen contents of below 0.1 ppm. Due to the fast reaction times of calcium thin-films, the measurements are performed under ambient conditions at 22°C and approx. 50% relative humidity. To keep fluctuations of the ambient climate to a minimum, all samples are measured consecutively in under an hour. For the WVTR measurement, each sample is taken from the glovebox individually and connected to a Keithley 2400 source measuring unit (SMU) (Keithley) in under 30 seconds. The SMU is connected to a measurement PC running a custom-made python program which performs a four point probe conductivity measurement with a set voltage of 20 mV every second. Measurements are done until complete calcium corrosion of each sample and generally takes between five to ten minutes. For more information on the electrical calcium test, see Klumbies et al.[26]

3. RESULTS AND DISCUSSION

In the following, we present the results on photolithographic patterning of single color phosphorescent *p-i-n* OLEDs using the bilayer approach. We demonstrate both, red and green OLEDs exhibiting comparable performance after the lift-off in HFEs to that of the reference devices defined by evaporation through the shadow mask (Sec.3.1). Next, we consider further steps required for integration of different color pixels on a planar substrate. We estimate the effect of air exposure and deposition of bilayer resist on non-encapsulated OLED devices, in terms of their electrical, optical and lifetime parameters (Sec.3.2).

3.1 Photo-patterning of Single Color Phosphorescent OLEDs

Large area OLED pixels (10.2 mm^2) were structured using photolithographic bilayer approach in order to guarantee a reliable comparison of device characteristics. Standard vacuum deposited red and green stacks defined via evaporation through shadow mask were used as a reference (**r0** and **g0**, respectively). Figure 3 shows the current-voltage-luminance (jVL) characteristics and external quantum efficiency (EQE) and luminous efficacy (LE) of the reference and the photo-patterned devices (**rP**, **gP**). It can be seen that both rP and gP show comparable jVL performance under forward and reverse bias operation (Fig.3(a)). Slight flattening of the jV curve is observed at higher current densities for a number of photo-patterned devices. This varied performance can be attributed to the morphological instability of certain organic films. Despite, emission properties of photo-patterned OLEDs are unaffected and both rP and gP reach EQE of 17.0% and 14.9% and LE of 28 lm/W and 57 lm/W at 1000 cd/m^2 without using additional light extraction structures, in line with state-of-the-art of the OLED technology. Further improvement in the device yield could be achieved by exchanging current n-transport layers with materials exhibiting high glass transition temperatures and low tendency to recrystallize.

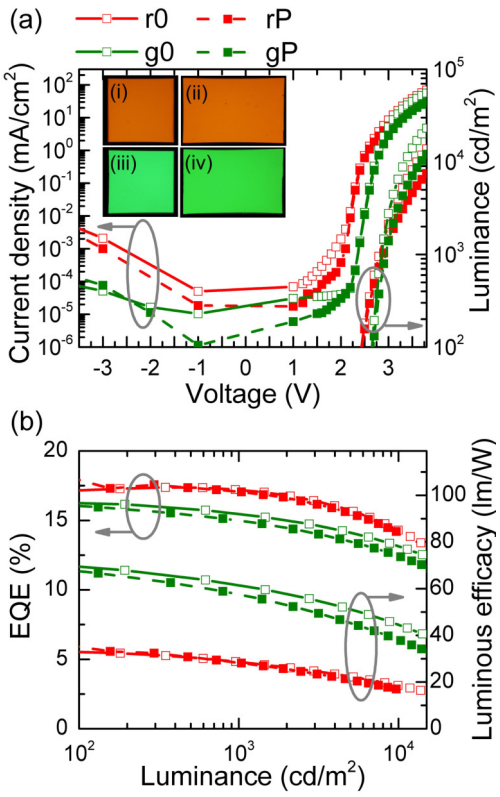

Figure 3. (a) Current density-voltage-luminance characteristics and (b) external quantum efficiency and luminous efficacy vs luminance of reference (r0, g0) and photo-patterned (rP, gP) devices. Insert in (a) shows microscope images of r0/g0 ((i)/(iii)) and rP/gP ((ii)/(iv)) pixels under electrical operation.

In order to achieve integration of three or more different OLED stacks on the same substrate, further processing steps and their influence on device performance have to be considered. In case of the proposed bilayer approach, repetition of the processes described in Sec.3.1 and Fig.1 would ultimately achieve the goal of multicolor patterning. However, several aspects different from the single color structuring have to be considered. First of all, unless the fabrication utilities are equipped with photolithographic tools operating in the inert atmosphere, the effect of the exposure of devices to ambient conditions for a limited amount of time have to be accounted for (a). Secondly, the fluoropolymer must be deposited and developed while being in direct contact with the OLED stack beneath (b). Besides, deposition and development of the imaging resist (c) together with baking of the resist at the elevated temperatures (d), plasma etching (e) and the UV exposure (f) might as well harm the OLED stack. In the next section, we focus on estimating the tolerance of the red OLEDs towards processing steps (a)-(c), *i.e.* exposure device to air and deposition/development of the bilayer resist.

3.2 Bilayer Processing on p-i-n OLEDs

After the deposition in vacuum, various additional treatments were performed on non-encapsulated red phosphorescent OLEDs. Afterwards, test samples were encapsulated as described in Sec.2.2 and their performance was compared to reference devices r0. Some of the OLEDs were exposed to ambient conditions for 4h (test device **r1**). Fluoropolymer layer was spin-coated on the test device **r2** in the inert N_2 atmosphere before 4h air exposure and then developed in HFE solvent. In addition to the fluoropolymer processing, imaging resist was spin-coated in the inert atmosphere and developed in air with TMAH based developer (samples **r3** (30min air exposure) and **r4** (4h air exposure)). Table 1 summarizes the treatment of the test devices.

Initial jVL characteristics of reference OLED r0 and test samples r1 and r2 are shown in Figure 4(a). It can be seen that the electrical performance of r1 under forward bias operation is comparable to the reference device. However, exposure to air results in the decrease of the initial luminance L_0, which is observed from the

onset of the emission and is increasingly more pronounced at higher luminance values. At a current density of $j = 100$ mA/cm^2, L_0 decreases from 18120±85 cd/m^2 for reference device r0 to 14690±950 cd/m^2 for r1. Comparison between r1 and r2 shows that additional fluoropolymer deposition and development does not alter device performance. This indicates that device exposure to the ambient conditions is the main factor affecting the OLED performance, while fluoropolymer processing is compatible with the OLED technology. Slight further drop in the initial luminance of r2 ($L_0 = 14090 \pm 950$ cd/m^2 at $j = 100$ mA/cm^2) is within the sample to sample variation range, and could be attributed to additional sample handling step.

Table 1. Samples tested for air exposure/bilayer processing. Fluoropolymer/imaging resist deposition and fluoropolymer development were performed in an inert atmosphere. Development of the imaging resist was done in the ambient conditions.

Sample name	**Description**	**Air exposure**	**Fluoropolymer processing**	**Imaging resist processing**
r0	reference	no	no	no
r1	air test	yes, 4h	no	no
r2	fluoropolymer test	yes, 4h	yes	no
r3	bilayer test (i)	yes, 30min	yes	yes
r4	bilayer test (ii)	yes, 4h	yes	yes

In order to compare long-term stability of the test devices, OLEDs were aged at constant current density of $j = 100$mA/cm^2. At such elevated current densities, various exciton annihilation mechanisms set in[27] and have to be considered to fully understand the degradation mechanism. However, since the device stack is kept constant throughout this work, we can attribute the changes in OLED performance of different test samples to the extrinsic factors, such as oxygen and moisture.[28,29]

Figure 4(b) shows luminance decay curves of devices r0, r1 and r2. Rapid decrease in luminance within the first several hours can be observed in all of the samples. Since Al cathode is porous to both oxygen and water,[30,31] initial drop in luminance is more pronounced in the samples r1 and r2, which were exposed to ambient conditions. This initial degradation is more pronounced in device r1, as indicated in the faster increase in the normalized luminance difference r1 and r0 ΔL_{r01} as compared to ΔL_{r02} (normalized luminance difference between r2 and r0) over the first hours of device operation.

A common practice to describe an OLED luminance decay over time $L(t)$ is to use combination of exponential decays[28,32] (Equation 1)

$$\frac{L(t)}{L0} = ae^{-k_{int}t} + be^{-k_{deg}t}, \tag{1}$$

where fitting parameters k_{int} and k_{deg} denote degradation rates of initial and monotonic decay, respectively, with corresponding amplitudes a and b. The lifetime LT90 is then estimated at a point where the initial luminance L_0 drops to 90% of its initial value. Since LT90 measured at the same current corresponds to different initial conditions for different samples, for better comparison, LT90 at a specific initial luminance can be extrapolated using Equation 2:

$$L0^n LT90 = const, \tag{2}$$

where n is the acceleration factor found empirically to be 2.2.[21] As shown in Figure 5, LT90 values extrapolated at $L_0 = 1000$ cd/m^2 drops from 810±150 h for reference sample to 401±75 h and 437±68 h for r1 and r2, respectively. This minor improvement in lifetime, together with slower initial increase and saturation of ΔL_{r02} indicates slight moisture barrier performance of the fluoropolymer layer. Electrical calcium tests (Ca-Tests) are performed to exclude OLED degradation by massive introduction of water into the device when using the imaging resist and to determine potential barrier qualities of the used spincoated materials. We find WVTRs of the fluoropolymer and bilayer resist to be 9.0±1.0 g/(m^{2}day) and 7.0±0.5 g/(m^{2}day), respectively. This indicates, that additional imaging resist deposition does not introduce additional moisture into the vicinity of fluoropolymer/Ca interface, but results in a slightly improved WVTR due to the increase in overall film thickness compared to a single fluoropolymer layer.

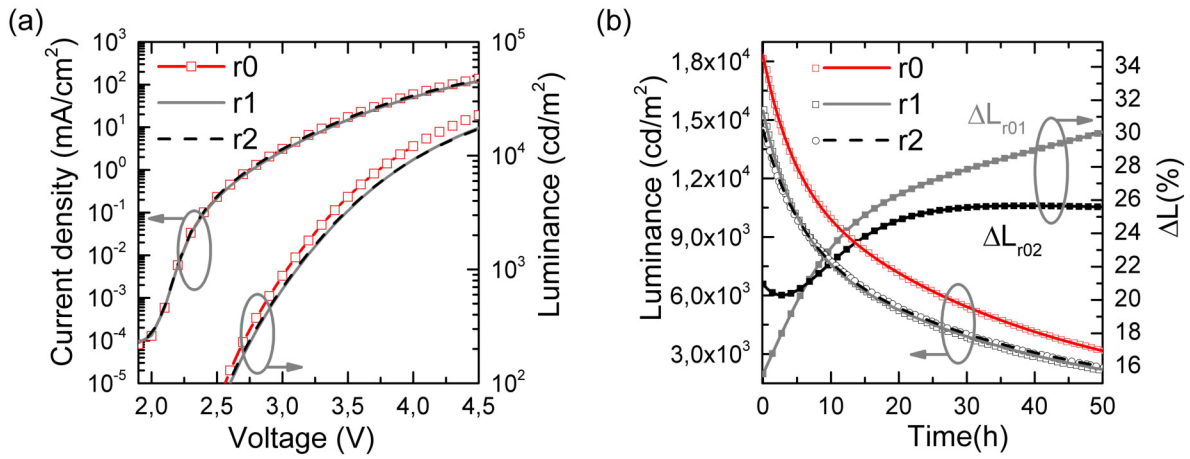

Figure 4. (a) Current density-voltage-luminance characteristics of reference (r0) and air exposed devices (r1 and r2). In between air exposure, additional fluoropolymer deposition and development were performed for sample r2. (b) Luminance decay curves of devices r0, r1 and r2 aged at 100 mA/cm^2. Solid lines represent exponential decay fits. ΔL_{r01} (ΔL_{r02}) denote normalized change in luminance between the reference device and r1 (r2).

Finally, we present the results on the full bilayer processing performed on the *p-i-n* OLED structure, including deposition and development of the imaging resist. Initial device performance is found to be severely diminished after 4h air exposure and bilayer processing. More than 5-fold decrease in both EQE and LE is observed, together with an increase by approx. 130mV in turn-on voltage, as compared to reference devices. However, the effect can be minimized significantly by reducing the time bilayer is in contact with the OLED stack. Devices kept in ambient conditions with fluoropolymer/imaging resist for 30min reach EQE of $13.08 \pm 2.11\%$ and LE of 18.40 ± 7.89lm/W at 1000cd/m^2. As can be seen from Fig.5 both L_0 and $LT90$ are as well highly reduced after the bilayer processing (samples r3 and r4) and are higher for the sample with a lower tact time. Measurement results are summarized in Table 2.

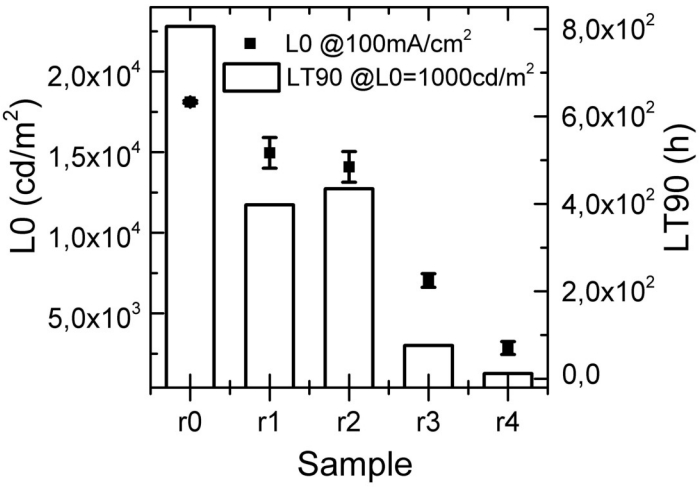

Figure 5. Initial luminance measured at 100 mA/cm^2 (black squares) and extrapolated device lifetime LT90 at $L_0 = 1000$ cd/m^2 of the tested samples.

The native solvent of the imaging resist is propylene glycol methyl ether acetate (PGMEA). Immersing of the OLED into the PGMEA results in a rapid destruction of the device. Considering this, together with Ca-test results and the pronounced dependence of OLED degradation on the time bilayer stays on the OLED structure, we attribute the degradation induced by the bilayer processing mainly to the diffusion of the PGMEA, which is introduced by the imaging resist, through the fluoropolymer layer and subsequent swelling of the active OLED layers.

Table 2. Accelerated degradation measurement of test devices. EQE and LE are measured at 1000cd/m^2, L_0 and LT90 are initial luminance and time at which luminance drops ato 90% to its initial value, respectively, measured at $j = 100$mA/cm^2. LT90* is extrapolated lifetime at $L_0 = 1000$cd/m^2

Sample name	**V***on***[V]**	**EQE[%]**	**LE[lm/W]**	**L$_0$[cd/m^2]**	**LT90[hours]**	**LT90*[hours]**
r0	2.35±0.06	16.98±1.45	27.75±2.50	18120±85	1.38±0.25	810±150
r1	2.38±0.05	14.98±0.87	23.50±1.47	14960±950	1.04±0.07	401±75
r2	2.33±0.05	13.68±0.81	21.88±1.49	14090±950	1.29±0.03	437±68
r3	2.40±0.04	13.08±2.11	18.40±7.89	7040±420	1.04±0.03	77±10
r4	2.48±0.03	3.03±0.45	4.08±0.66	2850±400	1.19±0.06	12.1±3.4

In summary, we have demonstrated that the bilayer structuring approach combining sacrificial fluoropolymer layer beneath imaging resist and lift-off in hydrofluoroethers enables photolithographic patterning of a single color OLEDs based on *p-i-n* device concept. Both, red- and green-emitting photopatterned devices reached external quantum efficiency of 17.0% and 14.9% and luminous efficacy of 28 lm/W and 57 lm/W at 1000 cd/m^2, respectively, in line with the state-of-the-art phosphorescent OLEDs structured via evaporation through the shadow mask. Additionally, we presented results on series of device treatment tests performed to elucidate main limiting factors for extending the proposed bilayer approach to the integration of the multicolored OLED arrays. Deposition of the fluoropolymer in direct contact with non-encapsulated *p-i-n* device and subsequent processing in HFE solvents were found to be compatible with the OLED technology. Besides, slight improvement in the long-term operation of the devices with deposited fluoropolymer layer exposed to air can be attributed to the moisture barrier properties of the deposited film. Finally, full bilayer processing was performed on *p-i-n* devices and it was shown to be detrimental to both initial and long-term performance of the OLEDs. Further research is focused on search for imaging resist with better compatibility with organic semiconductors as well as for polymers exhibiting better barrier properties combined with solubility in HFEs.

ACKNOWLEDGMENTS

The authors kindly acknowledge the financial support by the Free State of Saxony, the Sächsische Aufbaubank (SAB, Project Nr. 100087862), and the European Social Fund (ESF). This work was in parts sponsored by Fraunhofer Internal Programs under Grant Attract 162-600032.

REFERENCES

[1] Forrest, S. R., Baldo, M. A., OBrien, D. F., You, Y., Shoustikov, A., Sibley, S., and Thompson, M. E., "Highly efficient phosphorescent emission from organic electroluminescent devices," *Nature* **395**(6698), 151154 (1998).

[2] Reineke, S., Lindner, F., Schwartz, G., Seidler, N., Walzer, K., Lüssem, B., and Leo, K., "White organic light-emitting diodes with fluorescent tube efficiency," *Nature* **459**(7244), 234238 (2009).

[3] Forrest, S. R., "The path to ubiquitous and low-cost organic electronic appliances on plastic," *Nature* **428**(6986), 911918 (2004).

[4] Williams, G., Backhouse, C., and Aziz, H., "Integration of organic light emitting diodes and organic photodetectors for lab-on-a-chip bio-detection systems," *Electronics* **3**(1), 4375 (2014).

[5] Zang, Y., Zhang, F., Di, C.-a., and Zhu, D., "Advances of flexible pressure sensors toward artificial intelligence and health care applications," *Mater. Horiz.* (2014).

[6] Lochner, C. M., Khan, Y., Pierre, A., and Arias, A. C., "All-organic optoelectronic sensor for pulse oximetry," *Nature Communications* **5**, 5745 (2014).

[7] Schwartz, G., Tee, B. C.-K., Mei, J., Appleton, A. L., Kim, D. H., Wang, H., and Bao, Z., "Flexible polymer transistors with high pressure sensitivity for application in electronic skin and health monitoring," *Nature Communications* **4**, 1859 (2013).

[8] Biswas, S., Shalev, O., and Shtein, M., "Thin-film growth and patterning techniques for small molecular organic compounds used in optoelectronic device applications.," *Annu Rev Chem Biomol Eng* **4**, 289–317 (2013).

[9] Hwang, H. S., Zakhidov, A. A., Lee, J.-K., André, X., DeFranco, J. A., Fong, H. H., Holmes, A. B., Malliaras, G. G., and Ober, C. K., "Dry photolithographic patterning process for organic electronic devices using supercritical carbon dioxide as a solvent," *J. Mater. Chem.* **18**(26), 3087 (2008).

[10] Müller, C. D., Falcou, A., Reckefuss, N., Rojahn, M., Wiederhirn, V., Rudati, P., Frohne, H., Nuyken, O., Becker, H., and Meerholz, K., "Multi-colour organic light-emitting displays by solution processing," *Nature* **421**(6925), 829833 (2003).

[11] Deng, X. and Wong, K. Y., "Cross-linked conjugated polymers for achieving patterned three-color and blue polymer light-emitting diodes with multi-layer structures," *Macromolecular Rapid Communications* **30**(18), 15701576 (2009).

[12] Tian, P. F., Burrows, P. E., and Forrest, S. R., "Photolithographic patterning of vacuum-deposited organic light emitting devices," *Appl. Phys. Lett.* **71**(22), 3197 (1997).

[13] Lamprecht, B., Kraker, E., Weirum, G., Ditlbacher, H., Jakopic, G., Leising, G., and Krenn, J. R., "Organic optoelectronic device fabrication using standard UV photolithography," *physica status solidi (RRL) Rapid Research Letters* **2**(1), 1618 (2008).

[14] Taylor, P. G., Lee, J.-K., Zakhidov, A. A., Chatzichristidi, M., Fong, H. H., DeFranco, J. A., Malliaras, G. G., and Ober, C. K., "Orthogonal patterning of pedot:pss for organic electronics using hydrofluoroether solvents," *Advanced Materials* **21**(22), 23142317 (2009).

[15] Fong, H. H., Lee, J.-K., Lim, Y.-F., Zakhidov, A. A., Wong, W. W. H., Holmes, A. B., Ober, C. K., and Malliaras, G. G., "Orthogonal processing and patterning enabled by highly fluorinated light-emitting polymers," *Advanced Materials* **23**(6), 735739 (2010).

[16] Hansen, C. M., [*Hansen solubility parameters: a user's handbook*], CRC press (2012).

[17] Kleemann, H., Zakhidov, A., Anderson, M., Menke, T., Leo, K., and Lüssem, B., "Direct structuring of c60 thin film transistors by photo-lithography under ambient conditions," *Organic Electronics* **13**(3), 506513 (2012).

[18] Zakhidov, A. A., Lee, J.-K., Fong, H. H., DeFranco, J. A., Chatzichristidi, M., Taylor, P. G., Ober, C. K., and Malliaras, G. G., "Hydrofluoroethers as orthogonal solvents for the chemical processing of organic electronic materials," *Advanced Materials* **20**(18), 34813484 (2008).

[19] Zakhidov, A. A., Reineke, S., Lüssem, B., and Leo, K., "Hydrofluoroethers as heat-transfer fluids for OLEDs: Operational range, stability, and efficiency improvement," *Organic Electronics* **13**(3), 356360 (2012).

[20] Selzer, F., Weiß, N., Kneppe, D., Bormann, L., Sachse, C., Gaponik, N., Eychmüller, A., Leo, K., and Müller-Meskamp, L., "A spray-coating process for highly conductive silver nanowire networks as the transparent top-electrode for small molecule organic photovoltaics," *Nanoscale* (2015).

[21] Krotkus, S., Ventsch, F., Kasemann, D., Zakhidov, A. A., Hofmann, S., Leo, K., and Gather, M. C., "Photopatterning of highly efficient state-of-the-art phosphorescent OLEDs using orthogonal hydrofluoroethers," *Advanced Optical Materials* **2**(11), 10431048 (2014).

[22] Pfeiffer, M., Leo, K., Zhou, X., Huang, J., Hofmann, M., Werner, A., and Blochwitz-Nimoth, J., "Doped organic semiconductors: Physics and application in light emitting diodes," *Organic Electronics* **4**(2), 89–103 (2003).

[23] Furno, M., Meerheim, R., Hofmann, S., Lüssem, B., and Leo, K., "Efficiency and rate of spontaneous emission in organic electroluminescent devices," *Physical Review B* **85**(11), 115205 (2012).

[24] Paetzold, R., Winnacker, A., Henseler, D., Cesari, V., and Heuser, K., "Permeation rate measurements by electrical analysis of calcium corrosion," *Review of Scientific Instruments* **74**(12), 5147 (2003).

[25] Schubert, S., Klumbies, H., Müller-Meskamp, L., and Leo, K., "Electrical calcium test for moisture barrier evaluation for organic devices," *Review of Scientific Instruments* **82**(9), 094101 (2011).

[26] Klumbies, H., Müller-Meskamp, L., Nehm, F., and Leo, K., "Note: Influence of calcium corrosion on the performance of an adjacent permeation barrier," *Review of Scientific Instruments* **85**, 016104 (Jan 2014).

[27] Murawski, C., Leo, K., and Gather, M. C., "Efficiency roll-off in organic light-emitting diodes," *Advanced Materials* **25**(47), 6801–6827 (2013).

[28] Turak, A., "Interfacial degradation in organic optoelectronics," *RSC Advances* **3**(18), 6188–6225 (2013).

[29] Yamamoto, H., Brooks, J., Weaver, M. S., Brown, J. J., Murakami, T., and Murata, H., "Improved initial drop in operational lifetime of blue phosphorescent organic light emitting device fabricated under ultra high vacuum condition," *Appl. Phys. Lett.* **99**(3), 033301 (2011).

[30] Norrman, K., Larsen, N., and Krebs, F., "Lifetimes of organic photovoltaics: Combining chemical and physical characterisation techniques to study degradation mechanisms," *Solar Energy Materials and Solar Cells* **90**(17), 27932814 (2006).

[31] Hermenau, M., Riede, M., Leo, K., Gevorgyan, S. A., Krebs, F. C., and Norrman, K., "Water and oxygen induced degradation of small molecule organic solar cells," *Solar Energy Materials and Solar Cells* **95**(5), 12681277 (2011).

[32] Burrows, P., Bulovic, V., Forrest, S., Sapochak, L., McCarty, D., and Thompson, M., "Reliability and degradation of organic light emitting devices," *Applied Physics Letters* **65**(23), 2922–2924 (1994).